Multiscale modeling of microbial degradation of outer tissues of fiber-crop stems during the dew retting process

Gwenaëlle Lashermes, Laurent Bleuze, Sylvie Recous, Richard Voinot, François Lafolie, Brigitte Chabbert

Multiscale modeling of microbial degradation of outer tissues of fiber-crop stems during the dew retting process

Gwenaëlle Lashermes[a,*], Laurent Bleuze[a], Sylvie Recous[a], Richard Voinot[a], François Lafolie[b], Brigitte Chabbert[a]

[a]Université de Reims Champagne Ardenne, INRAE, FARE, 51100 Reims, France
[b]Université d'Avignon et des pays de Vaucluse, INRAE, EMMAH, 84000 Avignon, France

*Corresponding author: Gwenaëlle Lashermes, 2 esplanade Roland Garros, 51100 Reims, France, Tel.: 0033-326773582, gwenaelle.lashermes@inrae.fr

Keywords
Plant fiber
Aerobic biodegradation
Microbial kinetics
Dew retting
Multiscale modeling

Graphical abstract

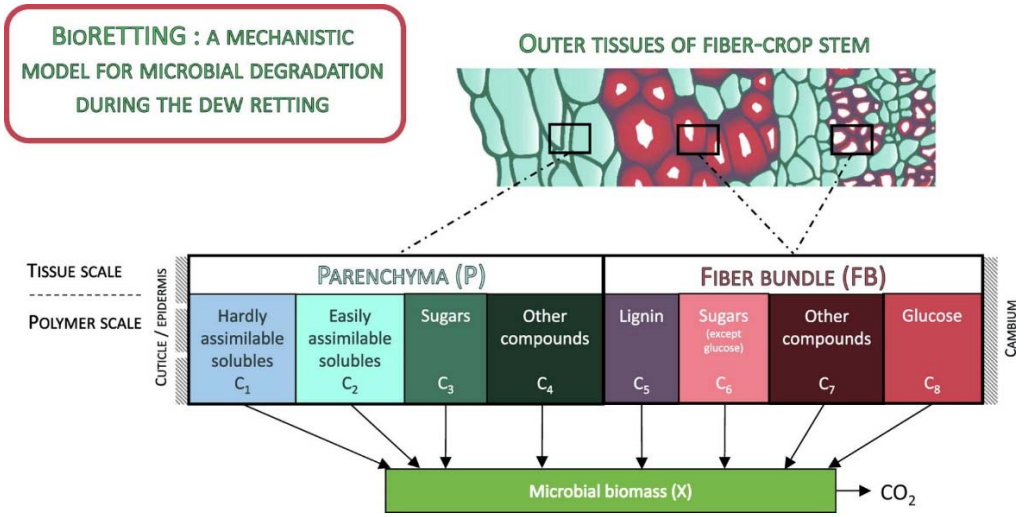

Abstract

Dew retting of fiber crops, such as hemp or flax, in the field after harvest promotes the microbial biodegradation of the tissues surrounding cellulosic fibers, which helps preserve the quality of fibers during their extraction and valorization for industry. This bioprocess is currently the bottleneck for plant fiber valorization because it is empirically managed and its controlling factors have not been properly quantified. A novel multiscale model representing tissue and polymer biodegradation was developed to simulate microbial growth on the stem during retting. The model was evaluated against experimental hemp retting data. It consistently simulated the mass loss of eight plant polymers belonging to two tissues of the stem outer layer, *i.e.,* parenchyma and fiber bundles. Microbial growth was modeled by Monod equations and modulated by the functions of temperature and moisture. This work provides a tool for gaining more insights into microorganism behavior during retting under local climate conditions.

Highlights

- A multiscale model of fiber-crop stem biodegradation during dew retting is proposed
- Mass loss dynamics were well simulated for outer tissues and individual polymers
- Median values of kinetic parameters from bioprocesses were relevant for retting
- Biodegradation was modulated by a moisture function to give consistent simulations
- The maximum specific growth rate optimized for hemp retting was 11.9 per day

Introduction

The substitution of fossil-based resources with plant biomass for synthon production, energy and materials is one of the main challenges facing the bioeconomy. Interest in fiber-reinforced materials has accelerated in recent years for applications in the construction and automotive industries, with flax and hemp being fiber crops of particular interest in Europe because they produce cellulosic fibers with low densities and good mechanical properties (Müssig, 2010). However, the quality of plant fibers is currently dependent on the extraction step as well as retting, a biological pretreatment based on microorganism action to degrade the bast tissues surrounding the long cellulosic fibers, in the stem outer layer (Liu et al., 2017). Retting facilitates the subsequent mechanical extraction of fibers and reduces the potential damage induced by this step. In Europe, dew retting of fiber crops is mostly performed atop the soil after harvest and under exposure to local environmental conditions with microorganisms naturally present in the field and at the plant surface. The main challenge of retting management is to accurately determine the duration of the process, which is partly influenced by local weather conditions, and to stop it when the bast fiber dissociates from the surrounding outer tissues and inner core while avoiding overretting, which can induce degradation of the bast fibers (Bourmaud et al., 2018). Although economical, retting is a complex bioprocess occurring in the field that needs to be managed and adapted to local conditions.

Modeling serves to describe our understanding of a process and is widely used as a tool to study the effect of different factors and environments on the dynamics of processes in the fields of biogeochemistry and biotechnology (Garnier et al., 2003; Mitchell et al., 2004). Modeling can also be applied to retting; however, this process has never been modeled to the best of our knowledge. Retting has similarities to some relatively more studied microbiological transformation processes, such as crop litter decomposition (Parton et al., 1988; Garnier et al., 2003), particularly when crop litter is left as mulch on the soil (Coppens et al., 2007), biomass solid-state fermentation (Mitchell et al., 1991; Tavares et al., 2006), and green waste composting (Zhang et al., 2012; Wang and Witarsa, 2016). These models propose various representations of the biodegradability of plant materials, distinguishing the intrinsic degradability of polymers and several representations of microbial growth dynamics. Models of crop litter decomposition include functions that modulate microbial activities such as temperature and moisture (Brisson et al., 2009; Manzoni et al., 2012).

However, compared to polymer-scale degradation models, one important feature needed for modeling retting is a tissue-scale representation of crop degradability. Indeed, outer stem tissues impacted by retting must be distinguished from the inner core of the stem, which is almost unaltered during dew-retting (Akin et al., 1996; Bleuze et al., 2018). Tissues are an ensemble of cells that may have their own degradation properties. Their degradability depends on factors beyond their individual polymer composition, such as the cell architectural arrangement (Bertrand et al., 2006), cell morphology (Wilson and Mertens, 1995), porosity (Zhang et al., 2018), and the presence of recalcitrant or hydrophobic compounds on accessible surfaces (Motte et al., 2015).

In addition, the time scale of retting is unique, i.e., a few weeks under field conditions distinguishes this process from other plant residue biodegradation processes. Field retting lasts longer than degradation in bioreactors, which takes place over a few hours to days and is much faster than litter decomposition in soil and litter composting, which last several months. At the retting time scale, small changes in moisture have a strong impact on the degradation rate (Nilsson and Karlsson, 2005).

The objective of this study was to develop a model describing biodegradation during the retting process, which was named the 'BioRETTING' model. BioRETTING is a mechanistic dynamic pool model that simulates the biodegradation of the outer layer of fiber crop stems at polymer and tissue scales and the microbial degradation of the substrate, modulated by abiotic conditions. The model was built to be generic for fiber-crop stems and to be able to take into account the morphological and chemical characteristics of stems, according to plant species and maturity stage. The aims of this work were to 1) integrate biodegradability criteria for the stem tissues, 2) combine the existing representation of microbial growth used in biotechnology models and the temperature and moisture functions used in agronomy, and 3) test the model against existing hemp retting data (Bleuze et al., 2018).

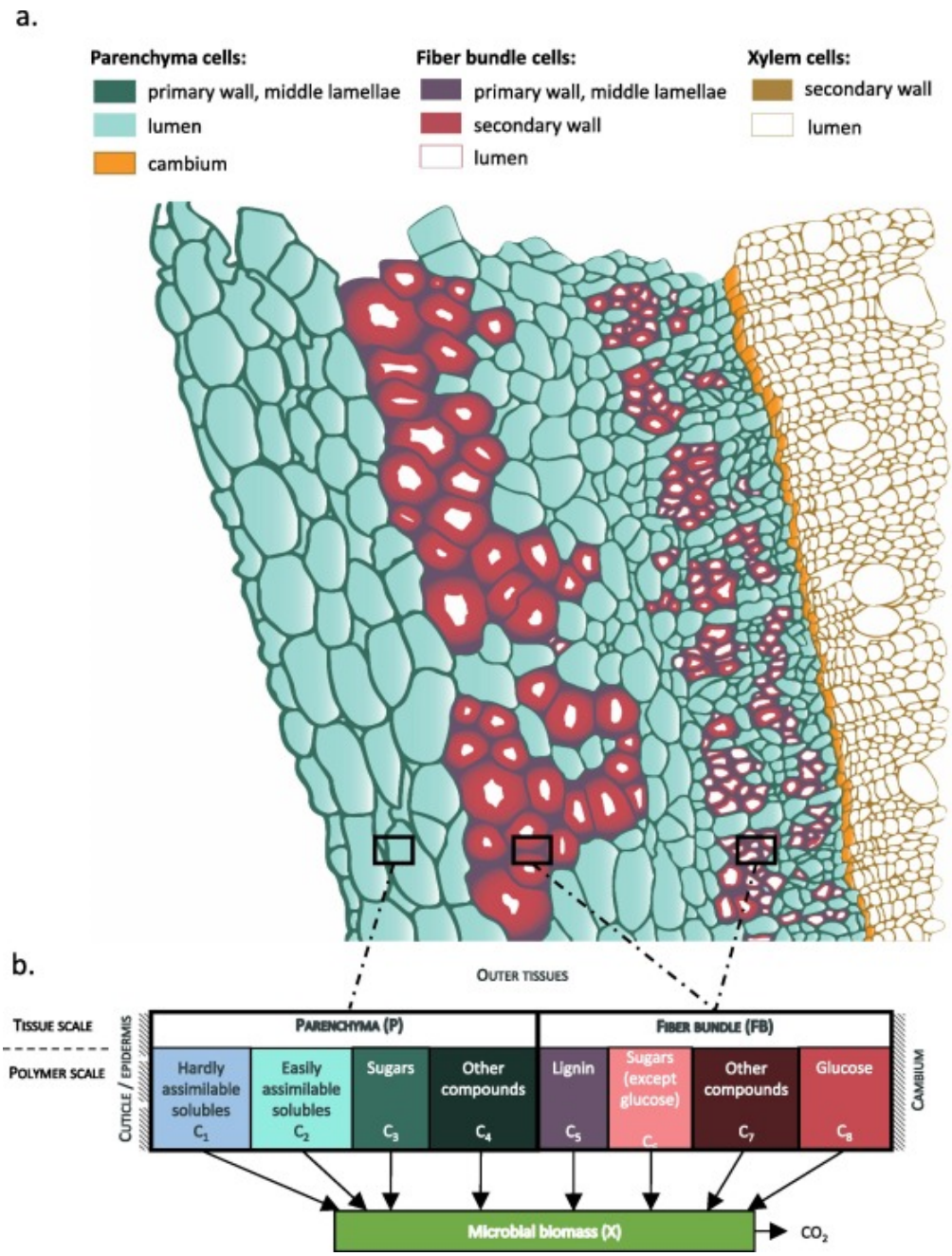

Figure 1. Representation of the outer tissues of fiber crops and their repartition in the diagram of the BioRETTING model. a) Schematic of a cross section of hemp showing the organization of the outer tissues, b) flow diagram of the simulation of changes in the outer tissue composition at the polymer and tissue scales via BioRETTING.

Materials and Methods

2.1. Substrate-microorganism system in retting and assumptions for major processes

2.1.1. Fiber-crop stems as a substrate during retting

Fiber-crop stems are mainly composed of inner tissues (xylem) and outer tissues separated by the cambium (undifferentiated cells) (Fig. 1a). The outer tissues are the main targets of microbial degradation during retting, in contrast to the inner tissues, which are not degraded during the few weeks of the retting process (Akin et al., 1996). In BioRETTING, we assumed that the highly lignified inner tissues were not colonized by microorganisms or altered, and we represented only the outer tissues of the stem.

To access the polymers of the outer tissues, microorganisms must pass the barriers of the cuticle and epidermis. The epidermis is a cell layer containing phenolic compounds and fatty compounds such as cutin and wax lipids forming cuticles at the outer surface (Heredia-Guerrero et al., 2014). These compounds, whose role is to protect living plants against invasion, are not easily biodegradable. We assumed that these compounds were not a source of energy for microorganisms that do not consume them but that rather seek openings in this barrier to allow their passage. Alternation between water evaporation under the effect of heat and rehumidification under the effect of rain and dew as well as photodegradation (Austin et al., 2016) may weaken the cuticle and epidermis and may cause cracks.

At the tissue scale, we divided the outer part of fiber-crop stems into two entities:

- The parenchyma and collenchyma (supporting tissues present in certain areas) and phloem (located between fibers and cambium) are made of cells whose lumen still contains cytosol and organelles at the beginning of retting. These cells have nonlignified primary walls and middle lamellae, mainly containing sugars, such as hemicelluloses, pectins and some nonoriented cellulose, forming a loose network. These cell walls also contain other compounds, such as structural proteins (Liu et al., 2015). These tissues form the first entity, which is easily biodegradable by microorganisms, with some of the soluble compounds of the cytoplasm being directly assimilated by microorganisms and other cell wall compounds becoming accessible after degradation by hydrolytic enzymes. The other soluble compounds of the cytoplasm are considered hardly biodegradable because they include some persistent organic nitrogen and phenolic compounds (Said-Pullicino et al., 2007). This representation was necessary to capture the dynamics of the soluble pools in the modeling of other biodegradation processes (Zhang et al., 2012; Lashermes et al., 2014). The soluble and cell wall compounds gathered in this first tissue entity, called "parenchyma" in the model, constitute the model pools. These pools constitute the polymeric scale of the model, as described in the diagram (Fig. 1b).
- The fiber bundle tissue is composed of thick-walled fibers that have lost their cytoplasmic contents, so their lumen is empty at fiber maturity. The cellulosic secondary cell walls are surrounded by lignified primary cell walls and middle lamellae. The fibers mainly contain oriented fibrils of crystalline cellulose associated with lower amounts of pectins, other hemicellulosic sugars, lignin, and other cell wall compounds, such as structural proteins (Kiyoto et al., 2018). Fiber bundles are inherently more difficult to degrade due to the loss of soluble cytoplasmic compounds, the crystallinity of cellulose fibers, and the protective effect of lignin, which is a recalcitrant phenolic polymer towards biodegradation and acts as a barrier against the biodegradation of other polymers (Himmel et al, 2007). The cell wall lignin content, tracked by the lignocellulosic index in the model, must be sufficiently high compared to other cell wall compounds to make it valuable for microorganisms to start its degradation (Moorhead et al., 2013). Indeed, below this threshold, the parenchyma compounds that are easier to access are in sufficient proportions to provide energy and nutrients to microorganisms, whereas above this threshold, lignin degradation becomes necessary for microorganisms. In the case of hemp, the outer tissues may also contain secondary fibers that are shorter and have smaller diameters than those of primary fibers. However, the structure and chemistry of secondary fibers are similar to those of the primary fiber bundles (Fernandez-Tendero et al., 2017; Kiyoto et al, 2018) and were represented in the same "fiber bundles" entity in the model.

Table 1. Variables, parameters and values used for the BioRETTING simulations

Symbol	Variables	Unit	Value	Simulation	Source[a]
C_1	soluble compounds of the parenchyma easy to assimilate	g 100 g^{-1} initial dry matter	18.5		[1]
C_2	soluble compounds of the parenchyma hard to assimilate	''	18.5		[1]
C_3	cell wall sugars of the parenchyma	''	11.5		[1]
C_4	cell wall other compounds of the parenchyma	''	2.9		[1]
C_5	cell wall lignin of the fiber bundle	''	2.5		[1]
C_6	cell wall sugars (except glucose) of the fiber bundle	''	7.5		[1]
C_7	cell wall other compounds of the fiber bundle	''	9.4		[1]
C_8	cell wall glucose of the fiber bundle	''	29.2		[1]
X	microbial biomass	''	0.8		[6]
CO_2	carbon dioxide gas from microbial degradation	''	0		[1]
P	parenchyma tissue	''	51.4		[1]
FB	fiber bundle tissue	''	48.6		[1]
	Parameters				
	K_S saturation constants				
K_{S1}	of C_1 by microbial biomass	''	500	A,B,C	[2]
K_{S2}	of C_2 by microbial biomass	''	10	A,B,C	[2]
K_{S3}	of C_3 by microbial biomass	''	37	A,B,C	[5]
K_{S4}	of C_4 by microbial biomass	''	37	A,B,C	[5]
K_{S5}	of C_5 by microbial biomass	''	500	A,B,C	[2]
K_{S6}	of C_6 by microbial biomass	''	37	A,B,C	[5]
K_{S7}	of C_7 by microbial biomass	''	37	A,B,C	[5]
K_{S8}	of C_8 by microbial biomass	''	300	A,B,C	[2]
μ_{max}	maximum specific growth rate for microbial biomass	d^{-1}	6.7	A,B	[5]
			11.9	C	[7]
Y	assimilation yield of microbial population	g biomass g^{-1} substrate	0.38	A,B,C	[5]
t_a [b]	time at the end of the exponential microbial growth phase	D	21	B	[6]
			8	C	[7]
L [b]	microbial survival factor at t_a	g survivor g^{-1} biomass	0.33	B,C	[5]
k [b]	exponential microbial decay constant	d^{-1}	0.63	B,C	[5]
LCI_T	threshold of the lignocellulose index of lignin control on microbial growth on fiber bundle	unitless	0.44	A,B,C	[2]
k_r	delay factor of the lignin control on microbial growth in fiber bundle	d^{-1}	0.2	A,B,C	[6]
T_{ref}	reference temperature	°C	15	A,B,C	[3]
θ_s	water content at saturation of plant tissues	g water g^{-1} DM	2.47	A,B,C	[8]
θ_{th}	water content at which microbial activity ceases	''	0.17	A,B,C	[4]
α	shape parameter of the moisture function f_W	unitless	2	A,B,C	[6]

[a][1] Bleuze et al., 2018; [2] Lashermes et al. 2014; [3] Brisson et al. 2009; [4] Bartholomew and Norman, 1947, [5] median values of the literature survey, [6] selected, [7] optimized in simulation C, [8] measured trough hemp stem immersion in water until saturation; [b]Parameters for modeling growth with Monod two-phase equation

2.1.2. Microorganism colonization and growth during retting

Generally, the microorganisms that colonize fiber-crop stems during dew retting come from soil (Djemiel et al., 2017; Ribeiro et al., 2015) but could also come from the phyllosphere and atmosphere (Lin et al., 2015). Microorganisms include fungi and bacteria (Ribeiro et al., 2015; Djemiel et al., 2017). Because we lack information on how to grasp the influence of microbial diversity in the model, we considered a single pool of microorganisms in the model. We found little data on microbial growth during retting. We assumed the microbial growth to be modeled with a Monod-type equation with a first phase of exponential microbial growth followed by a deceleration in growth marked by stationary phases, as it is frequently seen in composting (Zhang et al., 2012), solid-state fermentation (Mitchell et al., 2004), or yeast growth (Liu and Wu, 2008). Microbial growth during retting can be simulated with either Monod or Monod-two phase equations (Mitchell et al. 2004) in which a second phase is represented by a sudden deceleration in microbial growth when the outer tissues are observed to be completely colonized by microorganisms and when the fungal hyphae meet each other (Bleuze et al., 2018).

During the colonization and growth phases, microorganisms progressively form a biofilm on the stem surface between the epidermis and the parenchyma before progressing into the outer tissues (Bleuze et al., 2018; Fernando et al., 2019). Microorganisms grow by consuming soluble compounds, such as some of the cytoplasmic compounds that are easy to assimilate and still present in the plant cell at the time of cutting (Cotrufo et al., 2013) and polymeric compounds (cell wall polymers) that must be degraded to be assimilated. For this, microorganisms need to produce extracellular enzymes. Microbial cells produce metabolic waste, particularly CO_2. The proportion of CO_2 respired from the consumed substrate is represented in the model by an assimilation yield (Lashermes et al., 2016).

Microbial activity during retting is modulated by a temperature function developed for litter decomposition in soils (Brisson et al., 2009) and a moisture function developed for plant materials (Myrold et al., 1981; Manzoni et al., 2012).

2.2. Model framework

The model describes the dynamics of two pools at the tissue scale, the parenchyma (P) and fiber bundle (FB), which each are composed of the sum of four subpools of substrate defined at the polymeric scale (Fig. 1b). These variables are expressed in g C 100 g^{-1} initial dry matter (DM) (Table 1). The parenchyma subpools are soluble compounds that are easily (C_1) and hardly (C_2) assimilated by microorganisms, cell wall sugars (C_3), and other cell wall compounds (C_4), with $P = \sum_{i=1}^{4} C_i$. Among the fiber bundles, these subpools are lignin (C_5), cell wall sugars except glucose (C_6), other cell wall compounds (C_7), and fiber glucose (C_8), wherein $FB = \sum_{i=5}^{8} C_i$. The lignocellulose index (LCI) represents the lignin content (C_5) among the cell wall compounds (C_i, i=3-8) as follows:

$$LCI = {C_5}/{\sum_{i=3}^{8} C_i} \quad (1)$$

For LCI values lower than a threshold, LCI_T, a delay factor, k_r(d^{-1}), is applied to the degradation of cell wall substrates from fiber bundles with the aim of representing the degradation of fiber bundles, which may not be valuable for microorganisms compared to cell wall substrates from parenchyma, which are not protected by lignin. Beyond this threshold, the effect of the factor is null.

The growth of microbial biomass, μ_i, for each substrate C_i, follows Monod kinetics:

$$\begin{cases} \mu_i = \mu_{max} \cdot \frac{C_i}{K_{Si}+C_i} \cdot D \cdot f_T \cdot f_w \quad for \quad C_{i,i=1-4} \\ \mu_i = \mu_{max} \cdot \frac{C_i}{K_{Si}+C_i} \cdot k_r \cdot D \cdot f_T \cdot f_w \quad for \quad C_{i,i=5-8} \end{cases} \quad (2)$$

where K_{Si} (g C 100 g^{-1} initial DM) is the half-saturation constant of substrate i by microbial biomass, μ_{max} is the maximum specific growth rate for microbial biomass (d^{-1}), f_T is the temperature function, and f_W is the moisture function. D is the deceleration phase, defined as:

$$D = L \cdot \exp(-k \cdot (t - t_a)) \quad (3)$$

where t is the process time (d), t_a is the time at the end of the exponential growth phase (d), L is the microbial survival factor (g survivor g^{-1} total microbial biomass), and k is the exponential

constant of microbial decay (d^{-1}). D is used only when the model user selects the Monod-two phase equation and when $t < t_a$; otherwise, $D = 1$.

The dynamic of the total microbial biomass is described using the following equation:

$$dX/dt = \sum_{i=1}^{8} \mu_i \cdot X_i \quad (4)$$

where X_i is the portion of the total microbial pool growing on substrate C_i.

The decay of substrates 1-8 is described using the following equation:

$$dC_i/dt = -(1/Y) \cdot \mu_i \cdot X_i \quad (5)$$

with Y, the assimilated yield of the microbial biomass (g substrate assimilated g^{-1} degraded), balancing the assimilation and the formation of CO_2 as metabolic rejection.

The formation of CO_2 is represented by:

$$dCO_2/dt = (1 - Y)/Y \cdot \sum_{i=1}^{8} \mu_i \cdot X_i \quad (6)$$

The temperature effect on microbial growth is described by the logistic function calibrated for soil litter degradation by Brisson et al. (2009):

$$f_T = 25/[1 + 24 \cdot \exp\left(0.12 \cdot \left(T_{ref} - T\right)\right)] \quad (7)$$

where T_{ref} is a reference temperature equaling 15°C, T is the process temperature (°C). This function is very close to an Arrhenius function with an activation energy E_A=78 kj mol^{-1} K^{-1} between 0 and 35°C. The function is also equivalent to a Van't Hoff function between 0 and 25°C with a Q_{10} coefficient equal to 3.15, which makes it possible to simulate a relatively slower increase in microbial growth at high temperature. f_T ranges from 0.6 to 5 when T is 10 and 30°C, respectively, with f_T=1 when T=15°C (Fig. 2).

The effect of moisture on microbial growth is described by a logarithmic function as proposed by Manzoni et al. (2012) for water potential ψ (MPa) and expressed as a function of the moisture content θ (g g^{-1} DM), using the power function $\psi = 0.527 \cdot \theta^{-1.32}$ defined for crop litter (Myrold et al., 1981):

$$\begin{cases} f_W = 1 - \left(\dfrac{\ln\left(\theta_s/\theta\right)}{\ln\left(\theta_s/\theta_{th}\right)}\right)^{\alpha} \quad for\ \theta \geq \theta_{th} \\ f_W = 0 \quad for\ \theta < \theta_{th} \end{cases} \quad (8)$$

where θ_s is the crop moisture at saturation of the tissue sorption capacities, θ_{th}, is the moisture content at which microbial activity ceases, and α is a shape parameter.

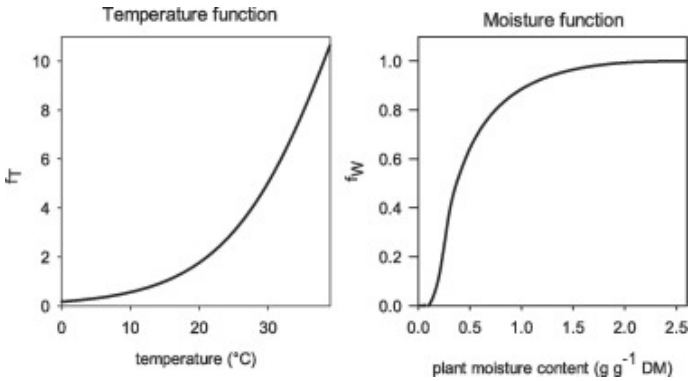

Figure 2. Temperature and moisture functions of the BioRETTING model

2.3. Experimental data for testing the BioRETTING module

The data collected by Bleuze et al. (2018) were used to test the model. Briefly, a retting experiment was conducted under laboratory conditions for 42 days at 15°C with hemp stems harvested at maturity, with controlled rain applied every week and chemical determination of the outer tissues over the retting process. The moisture content of the *plant material and dry mass loss were measured* during retting. The material carbon loss was used as a direct estimate of CO_2 evolution through mineralization for model testing because the carbon assimilated by the microbial biomass was measured with the remaining plant material.

2.4. Model initialization and measurability of the pools

The BioRETTING pools and subpools are all measurable, by microscopic imaging for analysis of tissue organization and by wet chemistry for the analysis of chemical compounds at the polymeric scale. However, the available data from wet chemical analyses corresponded to the entire outer tissues and not distinctly the fiber bundles and parenchyma (Bleuze et al., 2018). Available data were in g 100 g^{-1} DM, whereas 2D images giving information on the tissue surface were acquired in a different unit (in µm²). To achieve the repartitioning of chemical compound analyses among tissues, we attributed all of the measured soluble content to parenchyma and the measured lignin content to fiber bundles. For other cell wall

compound repartitions, the steps followed are briefly described (Fig. 3): the proportions of i) parenchyma and fiber bundles in the outer tissue surfaces, ii) cell wall and lumen within parenchyma, and iii) cell wall and lumen within fiber bundles were estimated based on i) 29 mosaic observations of half-stem cross sections obtained with a Leica TCS SP8 fluorescence confocal microscope (Leica Microsystems, Germany), ii) one observation with an Axioskop optical microscope (Zeiss, Germany), and iii) 4 confocal observations of red fluorescence.

Ten percent of the outer tissue surface was found to be attributable to the cell wall in the parenchyma and 35 ± 2% to the cell wall in the fiber bundles. Considering only cell wall compounds, 23% of these compounds are attributed to parenchyma and 77% to fiber bundles. It was assumed that the cell wall density was the same among parenchyma and fiber bundles, and the tissue organization was homogeneous among the outer tissues. We extrapolated the percent of the cell wall tissue surface (Fig. 3) to determine the quantities of cell wall chemicals. The rationale for this method can be illustrated with the following example. A cross-section selected to be representative of a homogeneous volume of outer tissues measuring 50 mm in height (value for hemp fiber length) was considered along with a density of the cell walls of, for example, 1.5 g cm^3, to be the same in parenchyma and fiber bundles (Thybring, 2017). For an observation of 1 mm of cambium length, the outer tissue surface was approximately 30,000 µm², among which parenchyma was 19,200 µm² (64%) and fiber bundles were 10,800 µm² (36%). The proportion of cell walls was 16% in the parenchyma and 96% in fiber bundles; thus, 3,072 µm² and 10,368 µm² were attributed to the cell walls in the parenchyma and fiber bundles, respectively. Considering a height of 50 mm and a density of 1.5 g cm^3, this corresponds to volumes of 153.6 10^6 μm^3 for parenchyma and 518.4 10^6 μm^3 for fiber bundles and to 230 µg and 778 µg of cell wall, respectively (i.e., 23% and 77% of the contents of cell wall compounds mentioned earlier).

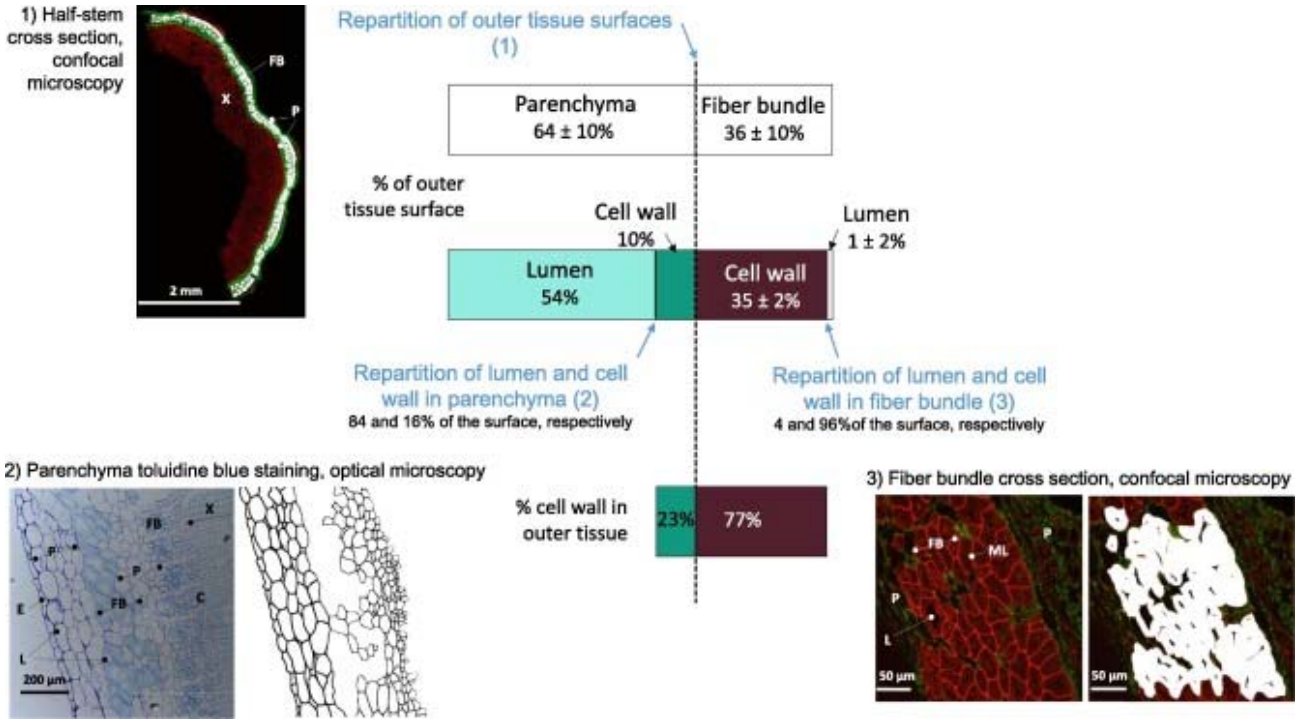

Figure 3. Methods used to repartition cell wall compounds analyzed in the outer tissues among parenchyma and fiber bundle tissues. Observations of hemp 1) half-stem cross sections to differentiate parenchyma and fiber bundle surfaces (confocal microscopy, objective x 10, 29 pictures, magnification x 100), 2) cross sections to differentiate the lumen and cell wall within the parenchyma (optical microscopy, toluidine blue coloration, 1 picture, magnification x 40), and (3) cross sections to differentiate the lumen and cell wall within fiber bundles (confocal microscopy, objective x40, 4 pictures, magnification x 400). E: epidermis; FB: fiber bundle; X: xylem; P: parenchyma; C: cambium; ML: middle lamella; L: lumen.

2.5. Values for parameters, temperatures and moisture functions

The median values for key parameters (μ_{max},Y, K_S, k, and L) used to perform the simulations were found from modeling studies of biotechnological processes using Monod kinetics: solid-state fermentation (Gelmi et al., 2002; Ikasari and Mitchell, 2000; van de Lagemaat et al., 2005; Liu et al., 2003; Mitchell et al. 1991; Montoya et al., 2015; Tavares et al., 2006), composting (Zhang et al., 2012), wastewater treatment (Liu et al., 2005), and aerobic growth of yeast (Dantigny, 1995; Liu and Wu, 2008; Tobajas and Garcia-Calvo, 2000; Zhang et al., 1997). Studies were retained in the literature survey when the parameters were expressed in the same units as those used in BioRETTING or when enough information was given to convert the value in the unit used. The median values for K_S were assigned to the cell wall compounds other than lignin and the oriented crystalline glucose of fiber bundles. The other values of K_S, as well as the parameter LCI_T, were selected from work on the decomposition of lignocellulosic substrate in soils using an equation close to the Monod equation (Lashermes et al., 2014). The value for θ_s was measured as the moisture content after which the stem particles do not absorb more water at a given temperature and humidity (Bartholomew and Norman, 1947). It was calculated as the difference between the initial weight of 5-cm of hemp stem particles determined at 40°C and the maximal wet weight after immersion in deionized water expressed per gram of dry hemp stem at 40°C and measured every 1-2 hours over a 30 hour experiment. The value for θ_{th} was found in the Bartholomew and Norman (1947) study on outer hemp tissues.

The moisture function was calculated daily based on the plant material moisture reported from the experiment, based on measures and extrapolations. During rain, plant material was assumed to absorb excess water equivalent to half of its maximum water retention, and then the plant water content decreased exponentially to reach the next observed value.

2.6. Implementation, calibration and evaluation of the model

The BioRETTING model was programmed in MATLAB (Mathworks, Natick, MA). The time step implemented was one hour to make it possible to use the hourly variation in moisture content during retting. The model program offers the possibility to calibrate parameters using the *fmincon* function of the MATLAB Optimization Toolbox (Mathworks, Natick, MA), which applies a sequential quadratic programming algorithm. The objective function is the total root mean square error (*RMSE*), defined as the sum of the values calculated between the experimental and simulated values of the eight variables (C_1+C_2, C_3, C_4, C_5, C_6, C_7, C_8, and CO_2). Two statistical criteria were used to evaluate the simulations. The coefficient of determination, R^2, and the mean difference, *MD*, were calculated as the sum of the differences between simulated and observed values. The model program and a tutorial are available (https://gitlab.com/farelab/teamgl/bioretting-model). The model is also implemented in the INRAE Virtual Soil Platform (https://www6.inrae.fr/vsoil) to facilitate coupling with other models.

Three simulations, with the parameter values described in Table 1, were performed as follows for testing the model: A) Monod kinetics was used to model microbial growth ($D = 1$ in eq. 2), B) Monod-two phase kinetics were used (eq. 2 and 3), C) Monod-two phase kinetics were used, and μ_{max} and t_a were optimized against the data of Bleuze et al. (2018) (simulation C).

Results and discussion

3.1. Modeling plant material biodegradation at the polymer and tissue scales

BioRETTING simulated the mass losses of substrate pools with a portion of the substrate removed transformed into microbial biomass (*X*) and the other consumed for cell function maintenance (CO_2) (Fig. 4). Simulations of the sum of parenchyma compounds (C1 to C4) at different retting stages were consistent with observations

corresponding to parenchyma tissue mass loss (R^2=0.97, 0.97 and 0.98 for simulations A, B, and C, respectively). The sum of fiber bundle compounds (C5 to C8) corresponding to the fiber bundle tissue mass loss was less well simulated (R^2 values=0.27, 0.69, and 0.61 for simulations A, B, and C, respectively). Monod and Monod-two phase kinetics produced simulations with a similar quality for parenchyma, whereas Monod-two phase kinetics produced the best simulations for fiber bundles. The sum of the RMSE values of all pool simulations for simulations A and B (3.05 and 3.11, respectively) decreased for simulation C to 2.72; thus, a moderate improvement was observed when μ_{max} and t_a were optimized. Negative values of *MD* were obtained, showing that the model overestimated the biodegradation rate of all compounds but underestimated that of other parenchyma compounds (C_4) while having a good fit for lignin (C_5).

The representation of the biodegradation of plant materials using several substrate pools at the polymeric scale has long been used in litter decomposition models. The plant substrates can be divided into metabolic (highly degradable) and structural (low degradable) pools (Parton et al., 1988) or into five pools of substrates with increasing recalcitrance to biodegradation (Garnier et al., 2003). This representation is also found in composting models with five pools (Zhang et al., 2012). BioRETTING describes eight pools at the polymeric scale. Nonetheless, in this study, similar K_{Si} parameter values were attributed to parenchyma sugars, fiber bundle sugars and other compounds, assuming the same intrinsic biodegradability. This saturation constant value at 37 g 100 g^{-1} initial DM was selected as the median value for noncrystalline glucose and lignocellulosic substrates from the literature (Mitchell et al. 1991, Zhang et al. 1997, Liu et al. 2005, Tavares et al. 2006, Zhang et al. 2012). A positive value of *MD* for C_3 indicates that K_{S3} must be higher for parenchyma sugars, and a negative value of *MD* for C_4 indicates that K_{S4} must be lower for other parenchyma than the selected value. The K_{Si} value of 300 g 100 g^{-1} initial DM was used for crystalline glucose from the fiber bundles, and 500 g 100 g^{-1} initial DM was used for lignin from the fiber bundles, as was done for lignocellulosic substrates (Lashermes et al., 2014). The lack of data for the lignocellulosic polymer saturation constant to individually parameterize these pools did not make it relevant to distinguish them from each other. However, this could be considered by making a greater experimental effort to determine the kinetics parameters for degradation of the individual compounds.

Models rarely take into account that individual compounds do not decompose independently from each other because they are interconnected. The effect of linkages between lignin and other polymers that hamper microbial enzyme accessibility to these polymers was introduced in BioRETTING as in a few decomposition models (Lashermes et al., 2014). A threshold in the cell-wall lignin content, expressed by the lignocellulosic index (LCI), marks the transition between two degradation steps: microorganisms consume in priority saccharides not shielded in lignin followed by lignin to release previously shielded saccharides (Moorhead et al., 2013).

In BioRETTING, tissues are not degrading at the same rate because fiber bundles contain lignin, which is mainly distributed in the middle lamella between the fibers, thus protecting the thick cellulosic secondary walls (Kiyoto et al., 2018). Authors showed different dynamics of lignocellulosic tissue biodegradation that suggest that criteria for resistance and for physical accessibility, specific for tissue entities, should be considered (Bertrand et al., 2006; Motte et al., 2015). Others proposed metrics at the tissue scale, such as cell wall thickness (Liu et al., 2015), that could be integrated into a model. The morphology of the cells also conditions the penetration of microorganisms to reach their substrate: the fibers are long cells closed at their ends and with little intercell communication, unlike parenchyma cells (Wilson and Mertens, 1995). In the present study, the empirical delay factor indexed to the LCI threshold aimed at modeling such differences appeared sufficient to reveal the observed differences in the two tissue degradation rates.

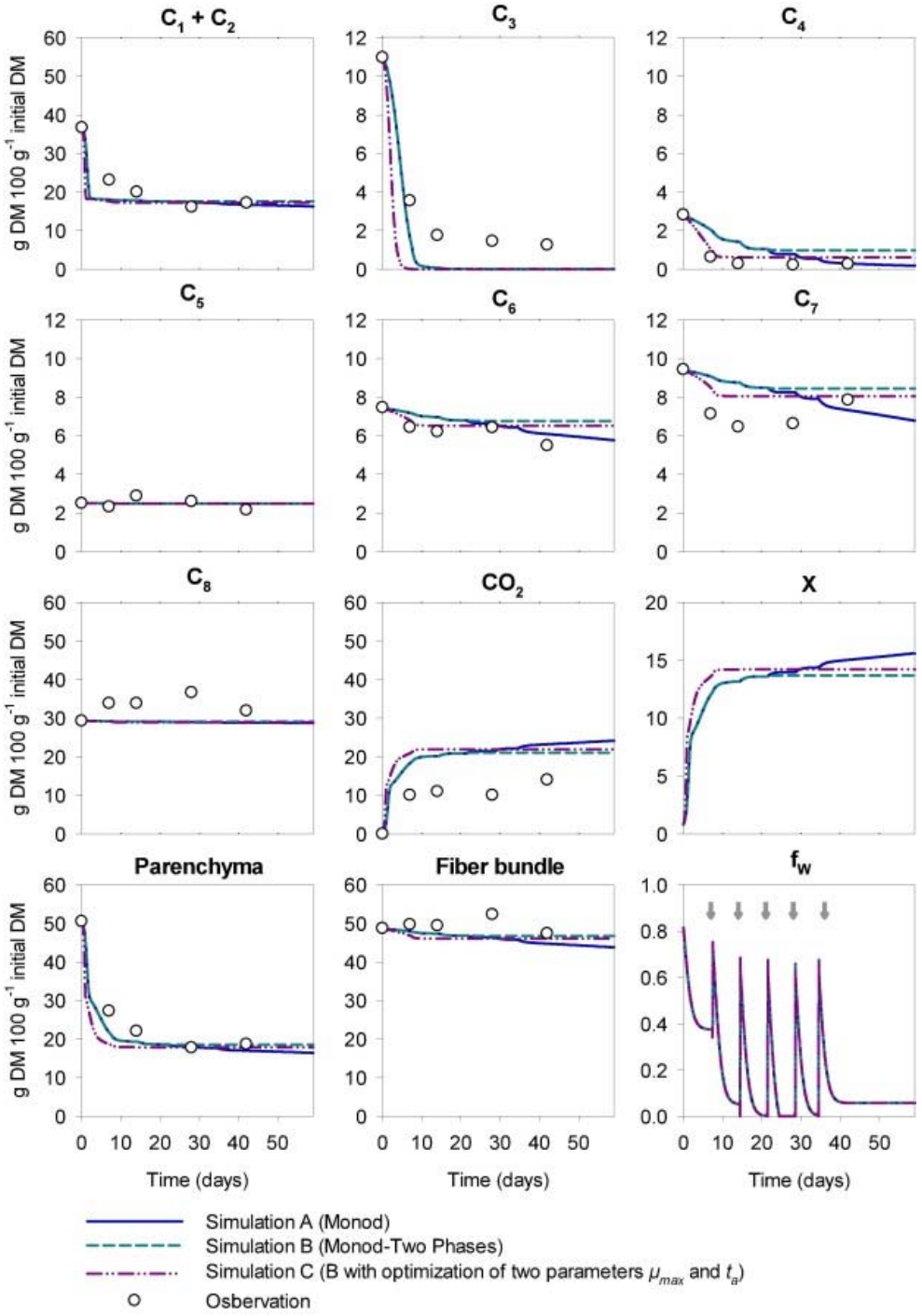

Figure 4. Observations and simulations performed with the BioRETTING model. Observed (symbols) and simulated (solid and dashed lines) data for chemical compounds (C_1+C_2, C_3, C_4, C_5, C_6, C_7, C_8), carbon dioxide (CO_2), parenchyma, fiber bundle tissues, and the simulated microbial biomass (X) and moisture function (f_W) during retting.

3.2. Modeling the microbial growth on plant material

The application of Monod kinetics in simulation A resulted in continual microbial growth and CO_2 respiration during retting that slowed down at regular intervals because of modulation by the moisture function (Fig. 4, see *CO_2*, *X,* and *f_W*). The experimental temperature corresponded to the reference temperature, so the temperature function had no influence on microbial growth. In the absence of modulation by moisture, the Monod kinetic produces a pattern of microbial growth with an exponential phase followed by a deceleration phase. The optimization of μ_{max} resulted in an increase in μ_{max} from 6.7 to 11.9 d^{-1} during the exponential growth phase. The optimized value obtained here for retting is within the range of values observed for other biotechnological processes. In simulations B and C, the application of Monod-two-phase kinetics resulted in a marked transition in the growth at t_a occurring after 21 days for simulation B and 8 days for simulation C (Fig. 4, see *X*). The deceleration term *D* (eq. 3) in the mathematical formula enables the microbial growth pattern to account for the second phase, where the decrease in growth is described by the survival factor and a constant for microbial decay (*L* and *k* parameters). This decrease can be due to competition between microorganisms, congestion of the medium, or local depletion in O_2 (Ikasari and Mitchell, 2000; Tavares et al., 2006). The optimization of $t_a$decreased its value from 21 to 8 days, shortening the time of intense biodegradation of all compounds due to exponential growth. The optimized value obtained for $t_a$was greater than the values of 1-3 days found for solid-state fermentation (Ikasari and Mitchell, 2000; Tavares et al., 2006). The values of *L* and *k* selected as the median values from the literature survey were very high (mostly *k*), which abruptly stopped growth. If the rain is more intense (i.e., f_W near 1), then the Monod kinetics could be more adapted to detect the optimum time to avoid overretting because the growth continues whereas it ceases with Monod-two phase kinetics. The only data set that we found for testing our model did not allow us to refine the calibration of these values. However since it consistently predicted the parenchyma and fiber bundles dynamics based on available observations, the model appears promising.

In comparison with soil decomposition models where the pattern of plant material breakdown is more commonly described with first-order kinetics affecting the C pools ($dC_i/\mathrm{dt} = -k_i \cdot C_i$, where C_i is the amount of substrate *i*, and k_i is the rate constant) (Parton et al., 1988), the use of the μ_i term (eq. 2) in the BioRETTING equations (Eq. 5, $dC_i/\mathrm{dt} = -(\mu_{max}/Y) \cdot X \cdot C_i/(\mathrm{K}_{Si} + C_i)$) constitutes an attempt to take account of microbial biomass growth. We opted for Monod-type kinetics, meaning that the microbial growth in this process is assumed to be limited by substrate saturation, as is usually used in biotechnology (Mitchell et al., 2004; Wang and Witarsa, 2016). A few other decomposition models simulate biodegradation by assuming that enzyme (or microbial biomass) saturation limits the process, using "reverse Michaelis-Menten" kinetics ($dC_i/\mathrm{dt} = -\mathrm{k}_i \cdot C_i \cdot X/(\mathrm{K}_M + \mathrm{X})$, with K_M the half-saturation constant for biomass on the substrate (Garnier et al., 2003). However, as long as the parameter values are chosen to make microbial activity the rate limiting process, these equations could have been applied because they produce similar patterns (Lashermes et al., 2014).

One pool of microorganisms was considered in BioRETTING, unlike a few other decomposition and composting models representing several degrading communities (Wang and Witarsa, 2016). Both bacteria and fungi are involved in the retting process; fungi are the first invaders and the main players during the early stages, and then bacteria outcompete the fungi, which constitute a nutrient source and migration pathway for bacteria that form biofilms. However, the few available observations have shown that fungi and bacteria have the same enzymatic capacities for pectinases, glucanases and cutinases (Fernando et al. 2019). These two groups of microorganisms therefore function

similarly with regard to their ability to degrade the substrate during retting, and the benefit of representing several pools of microorganisms in the model has not been established for this process. Potential differences could be observed in oxidative degradation capacities among these groups of microorganisms, but this has not yet been demonstrated during retting. In addition, swath turning carried out in the field during the process tends to homogenize microbial communities (Djemiel et al., 2017). Some studies have analyzed microbial diversity in fungal and bacterial communities during retting with genetic sequencing and have given relative abundances (Ribeiro et al., 2015; Djemiel et al., 2017) but have not quantified the size of microbial biomass needed for modeling. In this study, we estimated microbial respiration considering that mass was lost as CO_2; however, the inclusion of CO_2 or O_2 measurements based on infrared analyzers would greatly improve the model calibration. As expected, the moisture function strongly modulated microbial activity; thus, all kinetics had a low influence on the degradation for 1 day after each rain and then slowed down degradation as stems dried (see f_W in Fig. 4). We used the threshold value of 0.17 g water g^{-1} DM for microbial activity using the water saturated atmosphere proposed by Bartholomew and Norman (1947) for the same plant material (hemp outer tissues). For flax, Nilsson and Karlsson (2005) reported a fortiori that straw can be preserved for several years, exempt of microbial degradation if the moisture content is below 15% (wet basis), which would correspond to the same threshold used for hemp (17% dry basis). This threshold value is of paramount importance to predict the phases of microbial activity and cessation in retting dynamics. Because drying and wetting of plant materials have been reported to vary on an hourly basis during retting (Nilsson and Karlsson, 2005), the BioRETTING time step was chosen to be the hour, while the time step of models of microbial transformations is typically one day (Coppens et al., 2007; Tavares et al., 2006; Zhang et al., 2012). Once the water-stress threshold was exceeded, the shape parameter of 2 selected was in the higher range reported by Manzoni et al. (2012). The goal was to describe a strong increase in microbial activity after rain as the water content increased, translating the effect of moisture conservation within microbial biofilms at the stem surface during retting (Bleuze et al., 2018) (Fig. 2). Hence, according to the shape of the moisture function, relatively high microbial activity occurs at the moisture content at which approximately 2/3 of the water that can be retained by the plant material, and microbial activity decreases.

3.3. Model fiber-crop genericity and further needs for testing

The BioRETTING model was designed to be generic for flax and hemp and tested on hemp stem retting in the present study. A first order of magnitude for the parameter values has been proposed for this crop (see simulation C in Table 1). However, differences between flax and hemp exist, so the model should be tested on flax retting data to ensure its relevance. The cellulose in flax fibers may be more crystalline than that in hemp fibers, and the lignin distribution in the middle lamella within the fiber bundle is less homogeneous in flax (Bonatti et al., 2004), which can be taken into account with calibration work on flax data. Representation of tissues in three dimensions (3D) (Zoghlami et al., 2019) with additional implementation of polymer repartitioning could moreover help represent such heterogeneity. In the field, mechanical damage to stems from agricultural machinery that leads to additional openings in the cuticle barrier for microbial colonization is likely to vary with the harvesting stage, the agricultural equipment, and the morphology of the straw and potentially differ among hemp and flax. Model testing using field experiment data will also allow us to assess whether microbial colonization is adequately modeled in BioRETTING and to calibrate it for standard cultural practices, fiber-crop species and stage of maturity. This calibration step is essential before using the model to simulate the dynamics and duration of the retting process in interactions with the climatic conditions and to

explore different climatic and agronomic scenarios for hemp and flax cropping and retting systems.

Conclusions

BioRETTING is a novel and mechanistic model representing the biodegradation of polymers constituting the parenchyma and fiber-bundle tissues in the outer stem of fiber crops during dew retting. It consistently simulated a hemp retting experiment under controlled conditions using Monod or Monod-two phase kinetics and parameters equal to the median value from biotechnical processes. The fitted values for μ_{max} and t_a were 11.9 day^{-1} and 8 days, respectively, based on the experiment. Additional data are needed to continue modelling and improving the control of this process by considering the effect of environmental factors that affect microbial activity.

Acknowledgements

This work was supported by the Environment and Agronomy Division of INRAE and Reims Metropole within the framework of the MATRICE and RESIST projects. The authors thank F. Philippe for his technical assistance during this study.

CRediT author statement

Gwenaëlle Lashermes: Conceptualization, Methodology, Validation, Software, Writing - Original Draft, Supervision, Funding acquisition; **Laurent Bleuze:** Conceptualization, Methodology, Data Curation, Validation, Writing - Review & Editing; **Sylvie Recous**: Conceptualization, Methodology, Writing - Review & Editing, Funding acquisition; **Richard Voinot**: Methodology, Software, Writing - Review & Editing; **François Lafolie**: Software, Validation, Writing - Review & Editing ; **Brigitte Chabbert** : Conceptualization, Methodology, Writing - Review & Editing, Funding acquisition.

References

Akin, D.E., Gamble, G.R., Morrison Iii, W.H., Rigsby, L.L., Dodd, R.B. 1996. Chemical and Structural Analysis of Fibre and Core Tissues from Flax. *J. Sci. Food Agric.*, **72**(2), 155-165.

Austin, A.T., Mendez, M.S., Ballare, C.L. 2016. Photodegradation alleviates the lignin bottleneck for carbon turnover in terrestrial ecosystems. *Proc Natl Acad Sci U S A*, **113**(16), 4392-7.

Bartholomew, W.V., Norman, A.G. 1947. The Threshold Moisture Content for Active Decomposition of Some Mature Plant Materials 1. *Soil Sci. Soc. Am. J.*, **11**, 270–279.

Bertrand, I., Chabbert, B., Kurek, B., Recous, S. 2006. Can the biochemical features and histology of wheat residues explain their decomposition in soil? *Plant and Soil,* **281**(1-2), 291-307.

Bleuze, L., Lashermes, G., Alavoine, G., Recous, S., Chabbert, B. 2018. Tracking the dynamics of hemp dew retting under controlled environmental conditions. *Ind. Crop Prod.*, **123**, 55-63.

Bonatti, P.M., Ferrari, C., Focher, B., Grippo, C., Torri, G., Cosentino, C. 2004. Histochemical and supramolecular studies in determining quality of hemp fibres for textile applications. *Euphytica*, **140**(1), 55-64.

Bourmaud, A., Beaugrand, J., Shah, D.U., Placet, V., Baley, C. 2018. Towards the design of high-performance plant fibre composites. *Prog. Mater. Sci.*, **97**, 347-408.

Brisson, N., Launay, M., Mary, B., Beaudoin, N. 2009. Conceptual Basis, Formalizations and Parameterization of the Stics Crop Model. Quae, 304 p.

Coppens, F., Garnier, P., Findeling, A., Merckx, R., Recous, S. 2007. Decomposition of mulched versus incorporated crop residues: Modelling with PASTIS clarifies interactions between residue quality and location. *Soil Biol. Biochem.*, **39**(9), 2339-2350.

Cotrufo, M.F., Wallenstein, M.D., Boot, C.M., Denef, K., Paul, E. 2013. The Microbial Efficiency-Matrix Stabilization (MEMS) framework integrates plant litter decomposition with soil organic matter stabilization: do labile plant inputs form stable soil organic matter? *Glob Chang Biol*, **19**(4), 988-995.

Dantigny, P. 1995. Modeling of the aerobic growth of Saccharomyces cerevisiae on mixtures of glucose and ethanol in continuous culture. *J Biotechnol*, **43**(3), 213-20.

Djemiel, C., Grec, S., Hawkins, S. 2017. Characterization of Bacterial and Fungal Community Dynamics by High-Throughput Sequencing (HTS) Metabarcoding during Flax Dew-Retting. *Front Microbiol*, **8**, 2052.

Fernandez-Tendero, E., Day, A., Legros, S., Habrant, A., Hawkins, S., Chabbert, B. 2017. Changes in hemp secondary fiber production related to technical fiber variability revealed by light microscopy and attenuated total reflectance Fourier transform infrared spectroscopy. *Plos One*, **12**(6), e0179794.

Fernando, D., Thygesen, A., Meyer, A.S., Daniel, G. 2019. Elucidating Field Retting Mechanisms of Hemp Fibres for Biocomposites: Effects of Microbial Actions and Interactions on the Cellular Micro-morphology and Ultrastructure of Hemp Stems and Bast Fibres. *Bioressources* **14**(2), 38.

Garnier, P., Neel, C., Aita, C., Recous, S., Lafolie, F., Mary, B. 2003. Modelling carbon and nitrogen dynamics in a bare soil with and without straw incorporation. *Eur. J. Soil Sci.*, **54**(3), 555-568.

Gelmi, C., Pérez-Correa, R., Agosin, E. 2002. Modelling Gibberella fujikuroi growth and GA3 production in solid-state fermentation. *Process Biochem*, **37**(9), 1033-1040.

Heredia-Guerrero, J.A., Benitez, J.J., Dominguez, E., Bayer, I.S., Cingolani, R., Athanassiou, A., Heredia, A. 2014. Infrared and Raman spectroscopic features of plant cuticles: a review. *Front Plant Sci*, **5**, 305.

Himmel, M.E., Ding, S.Y., Johnson, D.K., Adney, W.S., Nimlos, M.R., Brady, J.W., Foust, T.D. 2007. Biomass recalcitrance: engineering plants and enzymes for biofuels production. *Science,* **315**(5813), 804-7.

Ikasari, L., Mitchell, D.A. 2000. Two-phase model of the kinetics of growth of Rhizopus oligosporus in membrane culture. *Biotechnol Bioeng*, **68**(6), 619-627.

Kiyoto, S., Yoshinaga, A., Fernandez-Tendero, E., Day, A., Chabbert, B., Takabe, K. 2018. Distribution of Lignin, Hemicellulose, and Arabinogalactan Protein in Hemp Phloem Fibers. *Microsc Microanal*, **24**(4), 442-452.

Lagemaat, J.v.d., Pyle, D.L. 2005. Modelling the uptake and growth kinetics of Penicillium glabrum in a tannic acid-containing solid-state fermentation for tannase production. *Process Biochem*, **40**(5), 1773-1782.

Lashermes, G., Moorhead, D., Recous, S., Bertrand, I. 2014. Interacting Microbe and Litter Quality Controls on Litter Decomposition: A Modeling Analysis. *Plos One*, **9**(9).

Lashermes, G., Gainvors-Claisse, A., Recous, S., Bertrand, I. 2016. Enzymatic Strategies and Carbon Use Efficiency of a Litter-Decomposing Fungus Grown on Maize Leaves, Stems, and Roots. *Front Microbiol*, **7**(1315).

Lin, Y., He, X., Ma, T., Han, G., Xiang, C. 2015. Priority colonization of Cinnamomum camphora litter by endophytes affects decomposition rate, fungal community and microbial activities under field conditions. *Pedobiologia*, **58**(5), 177-185.

Liu, J.-Z., Weng, L.-P., Zhang, Q.-L., Xu, H., Ji, L.-N. 2003. A mathematical model for gluconic acid fermentation by Aspergillus niger. *Biochem. Eng. J.*, **14**(2), 137-141.

Lui, L., Zhiping, W., Jie, Y., Xiaojun, S., Weimin, C. 2005. Investigation on the formation and kinetics of glucose-fed aerobic granular sludge. *Enzyme Microb. Technol.*, **36**(4), 487-491.

Liu, Y.S., Wu, J.Y. 2008. Modeling of Xanthophyllomyces dendrorhous growth on glucose and overflow metabolism in batch and fed-batch cultures for astaxanthin production. *Biotechnol Bioeng*, **101**(5), 996-1004.

Liu, M., Fernando, D., Meyer, A.S., Madsen, B., Daniel, G., Thygesen, A. 2015. Characterization and biological depectinization of hemp fibers originating from different stem sections. *Ind. Crop Prod.*, **76**, 880-891.

Liu, M., Thygesen, A., Summerscales, J., Meyer, A.S. 2017. Targeted pre-treatment of hemp bast fibres for optimal performance in biocomposite materials: A review. *Ind. Crop Prod.*, **108**, 660-683.

Manzoni, S., Schimel, J.P., Porporato, A. 2012. Responses of soil microbial communities to water stress: results from a meta-analysis. *Ecology*, **93**(4), 930-938.

Mitchell, D.A., Do, D.D., Greenfield, P.F., Doelle, H.W. 1991. A semimechanistic mathematical model for growth of Rhizopus oligosporus in a model solid-state fermentation system. *Biotechnol Bioeng*, **38**(4), 353-62.

Mitchell, D.A., von Meien, O.F., Krieger, N., Dalsenter, F.D.H. 2004. A review of recent developments in modeling of microbial growth kinetics and intraparticle phenomena in solid-state fermentation. *Biochem. Eng. J.*, **17**(1), 15-26.

Montoya, S., Sánchez, Ó.J., Levin, L. 2015. Mathematical Modeling of Lignocellulolytic Enzyme Production from Three Species of White Rot Fungi by Solid-State Fermentation. Cham. Springer International Publishing. pp. 371-377.

Moorhead, D.L., Lashermes, G., Sinsabaugh, R.L., Weintraub, M.N. 2013. Calculating co-metabolic costs of lignin decay and their impacts on carbon use efficiency. *Soil Biol. Biochem.*, **66**, 17-19.

Motte, J.C., Watteau, F., Escudie, R., Steyer, J.P., Bernet, N., Delgenes, J.P., Dumas, C. 2015. Dynamic observation of the biodegradation of lignocellulosic tissue under solid-state anaerobic conditions. *Bioresour Technol*, **191**, 322-6.

Müssig, J., 2010. Industrial Applications of Natural Fibres: Structure, Properties and Technical Applications, John Winley & Sons, 560p.

Myrold, D.D., Elliott, L.F., Papendick, R.I., Campbell, G.S. 1981. Water Potential-Water Content Characteristics of Wheat Straw1. *Soil Sci Soc Am J.*, **45**(2), 329-333.

Nilsson, D., Karlsson, S. 2005. A Model for the Field Drying and Wetting Processes of Cut Flax Straw. *Biosyst. Eng.*, **92**(1), 25-35.

Parton, W.J., Stewart, J.W.B., Cole, C.V. 1988. Dynamics of C, N, P and S in grassland soils - a model. *Biogeochemistry*, **5**(1), 109-131.

Ribeiro, A., Pochart, P., Day, A., Mennuni, S., Bono, P., Baret, J.L., Spadoni, J.L., Mangin, I. 2015. Microbial diversity observed during hemp retting. *Appl Microbiol Biotechnol*, **99**(10), 4471-84.

Said-Pullicino, D., Erriquens, F.G., Gigliotti, G. 2007. Changes in the chemical characteristics of water-extractable organic matter during composting and their influence on compost stability and maturity. *Bioresour Technol*, **98**(9), 1822-1831.

Tavares, A.P.M., Coelho, M.A.Z., Agapito, M.S.M., Coutinho, J.A.P., Xavier, A.M.R.B. 2006. Optimization and modeling of laccase production by Trametes versicolor in a bioreactor using statistical experimental design. *Appl. Biochem. Biotechnol.*, **134**(3), 233-248.

Thybring, E.E. 2017. Water relations in untreated and modified wood under brown-rot and white-rot decay. *Int Biodeterior Biodegradation*, **118**, 134-142.

Tobajas, M., Garcia-Calvo, E. 2000. Comparison of analysis methods for determination of the kinetic parameters in batch cultures. *World J Microbiol Biotechnol*, **16**(8), 845-851.

Wang, Y., Witarsa, F. 2016. Application of Contois, Tessier, and first-order kinetics for modeling and simulation of a composting decomposition process. *Bioresour Technol*, **220**, 384-393.

Wilson, J. R.; Mertens, D. R., 1995. Cell Wall accessibility and cell structure limitations to microbial digestion of forage. *Crop Science*, **35**, 251-259.

Zhang, H., Li, J., Huang, G., Yang, Z., Han, L. 2018. Understanding the synergistic effect and the main factors influencing the enzymatic hydrolyzability of corn stover at low enzyme loading by hydrothermal and/or ultrafine grinding pretreatment. *Bioresour Technol*, **264**, 327-334.

Zhang, Y., Lashermes, G., Houot, S., Doublet, J., Steyer, J.P., Zhu, Y.G., Barriuso, E., Garnier, P. 2012. Modelling of organic matter dynamics during the composting process. *Waste Manag*, **32**(1), 19-30.

Zhang, Z., Scharer, J.M., Moo-Young, M. 1997. Mathematical model for aerobic culture of a recombinant yeast. *Bioprocess Eng.*, **17**(4), 235-240.

Zoghlami, A., Refahi, Y., Terryn, C., Paës, G. 2019. Multimodal characterization of acid-pretreated poplar reveals spectral and structural parameters strongly correlate with saccharification. *Bioresour Technol*, **293**, 122015.

Supplementary information

Figure S1. Dynamics of the hemp moisture content during retting used to initialize the moisture function (Bleuze et al., 2018)

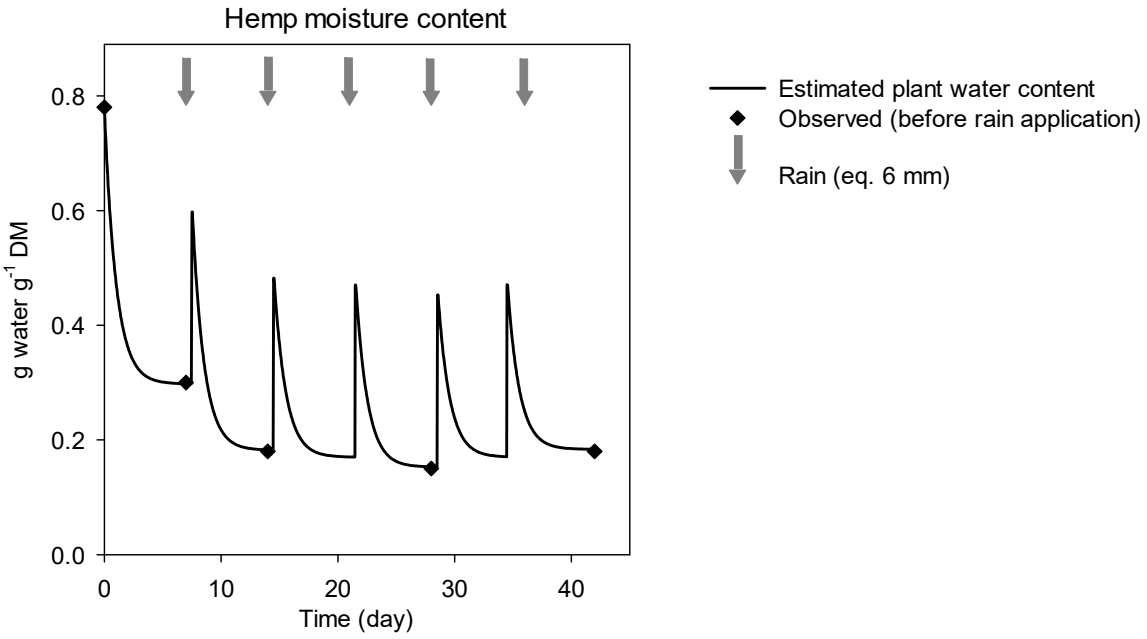

Figure S2. Observations and simulations performed with the BioRETTING model with no influence of the moisture function ($f_W = 1$). Observed (symbols) and simulated (solid and dashed lines) data of chemical compounds (C_1+C_2, C_3, C_4, C_5, C_6, C_7, C_8, and carbon dioxide (CO_2)), parenchyma, fiber bundle tissues, and simulated microbial biomass (X) during retting.

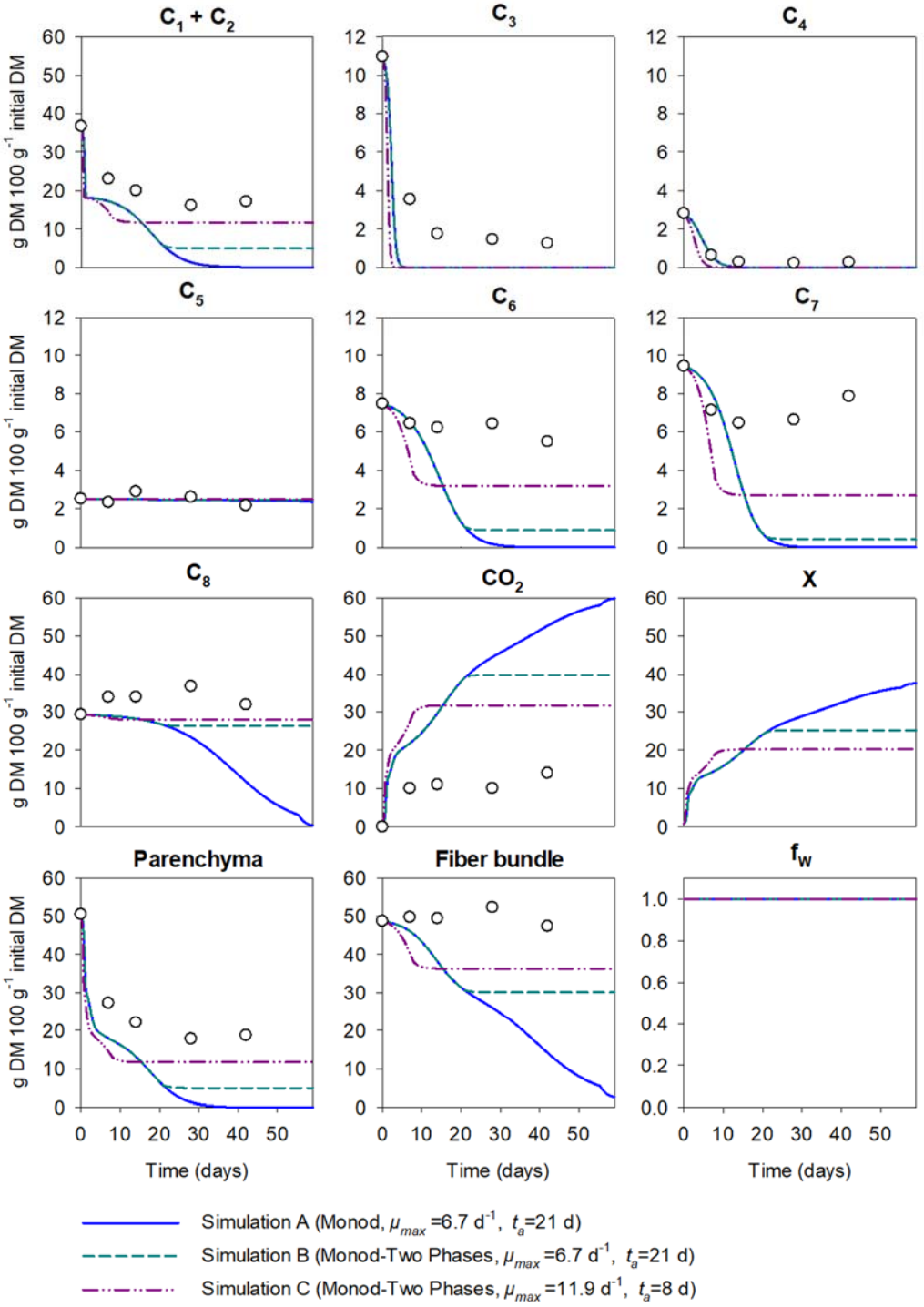

Table S1. Initial experimental chemical contents of the outer tissue of the hemp stem and repartitioning in the outer tissues (Bleuze et al. 2018)

Compounds		Observations			Simulations	
		Outer tissues	Parenchyma	Fiber bundle	Parenchyma	Fiber bundle
			g 100 g^{-1} dry matter			
Total (Initial)			51.5	48.5		
	Soluble	*37.0*	*37.0*	*0.0*		
	Glucose	*38.4*	*9.2*	*29.2*		
	Other sugars	*9.8*	*2.3*	*7.5*		
	Lignin	*2.5*	*0.0*	*2.5*		
	Others	*12.3*	*2.9*	*9.4*		
	Cell wall (total)	*63.0*	*14.5*	*48.5*		
Total (Day 7)			27.3	49.7	21.7	47.9
					21.7	47.9
					18.7	46.8
Total (Day 14)			22.0	49.4	19.3	47.3
					19.3	47.3
					17.9	46.0
Total (Day 28)			17.8	52.3	18.2	46.4
					18.6	46.7
					17.9	46.0
Total (Day 42)			18.7	47.4	17.0	44.7
					18.6	46.7
					17.9	46.0

Table S2. Key model kinetic parameters surveyed in the literature concerning biotechnical processes and their medians used for simulations

Microorganisms	Substrate (C source)	Microbial growth equation	μ_{max}	Y	K_S	k	L	Reference
Solid-state fermentation			d^{-1}	g biomass g^{-1} substrate	g 100 g^{-1} initial substrate	d^{-1}	g survivor g^{-1} biomass	
Rhizopus oligosporus	glucose	Monod[a]	14.4	0.40	18			Mitchell et al. 1991
''	glucose	Monod-two phases[b]	51.6			1.73	0.14	Ikasari and Mitchell 2000
''	lignocellulosic substrate	Monod-two phases	14.4			1.01	0.29	Ikasari and Mitchell 2000
Trametes versicolor	glucose	Monod-two phases	0.9	0.17	47	0.09	0.37	Tavares et al. 2006
''	medium without glucose	Monod-two phases	0.8	0.38		0.25	0.41	Tavares et al. 2006
Aspergilus niger	glucose	Monod-logistic[c]	5.3	0.10				Liu et al. 2003
Coriolus versicolor	lignocellulosic substrate	Monod-logistic	6.7					Montoya et al. 2015
Penicillium glabrum	glucose	Monod-logistic	4.1	0.34				van de Lagemaat et al. 2005
Gibberella fujikuroi	Starch	Monod-logistic	13.7	0.24				Gelmi et al. 2002
Composting								
Mixed microbiota	lignocellulosic substrate	Monod	6.0	0.50	101			Zhang et al. 2012
Wastewater treatment								
Mixed microbiota	glucose	Monod	13.2	0.21	37			Liu et al. 2005
Aerobic growth of yeast		Monod						
Saccharomyces cerevisiae	glucose and ethanol	Monod	10.8	0.48				Dantigny 1995
''	glucose	Monod	6.0	0.48	0.05			Zhang et al. 1997
Candida utilis	glucose	Monod	7.2	0.55	1-13			Tobajas and Garcia-Calvo 2000
Xanthophyllomyces dendrorhous	glucose and ethanol	Monod	3.1	0.37				Liu and Wu 2008
		Median	**6.7**	**0.38**	**37**	**0.63**	**0.33**	

[a] $dX/dt = \mu \cdot X$; [b] $dX/dt = \mu \cdot X$ for $t < t_a$ and $dX/dt = \mu \cdot X \cdot L \cdot \exp(-k \cdot (t - t_a))$ for $t \geq t_a$; [c] $dX/dt = \mu \cdot X\,(1 - X/X_m)$ with $\mu = \mu_{max} \cdot \frac{C}{K_S + C}$; X_m is the maximum microbial biomass

Table S3. Statistical evaluation of the three simulations

		Simulations		
		A (Monod)	B (Monod-two phases)	C (B with optimization of two parameters)
RMSE	C_1+C_2	0.15	0.15	0.15
	C_3	0.10	0.11	0.06
	C_4	0.32	0.37	0.20
	C_5	0.41	0.43	0.41
	C_6	0.26	0.33	0.24
	C_7	0.54	0.50	0.32
	C_8	0.64	0.64	0.66
	Parenchyma	0.10	0.10	0.09
	Fiber bundle	0.74	0.69	0.80
	CO_2	0.61	0.58	0.67
	Total	**3.05**	**3.11**	**2.72**
MD	C_1+C_2	-2.1	-2.0	-2.1
	C_3	-0.8	-1.0	-0.6
	C_4	0.7	0.8	0.5
	C_5	-0.1	-0.1	-0.1
	C_6	0.1	0.3	-0.1
	C_7	0.6	0.9	0.4
	C_8	-6.0	-6.0	-6.4
	Parenchyma	-2.2	-5.0	-2.2
	Fiber bundle	-5.4	-5.0	-6.1
	CO_2	7.6	7.1	8.3
R^2	C_1+C_2	0.93	0.93	0.93
	C_3	0.98	0.99	1.00
	C_4	0.72	0.82	0.97
	C_5	0.00	0.09	0.07
	C_6	0.52	0.36	0.51
	C_7	0.00	0.17	0.52
	C_8	0.40	0.78	0.78
	Parenchyma	0.97	0.97	0.98
	Fiber bundle	0.27	0.69	0.61
	CO_2	0.96	0.93	0.91
	Mean	**0.58**	**0.67**	**0.73**